



HAL
open science

Wind Turbine Quantification and Reduction of Uncertainties Based on a Data-Driven Data Assimilation Approach

Adrien Hirvoas, Clémentine Prieur, Élise Arnaud, Fabien Caleyron, Miguel Munoz Zuniga

► **To cite this version:**

Adrien Hirvoas, Clémentine Prieur, Élise Arnaud, Fabien Caleyron, Miguel Munoz Zuniga. Wind Turbine Quantification and Reduction of Uncertainties Based on a Data-Driven Data Assimilation Approach. *Journal of Renewable and Sustainable Energy*, 2022, 14 (5), pp.053303. 10.1063/5.0086255 . hal-03855143

HAL Id: hal-03855143

<https://hal-ifp.archives-ouvertes.fr/hal-03855143>

Submitted on 16 Nov 2022

HAL is a multi-disciplinary open access archive for the deposit and dissemination of scientific research documents, whether they are published or not. The documents may come from teaching and research institutions in France or abroad, or from public or private research centers.

L'archive ouverte pluridisciplinaire **HAL**, est destinée au dépôt et à la diffusion de documents scientifiques de niveau recherche, publiés ou non, émanant des établissements d'enseignement et de recherche français ou étrangers, des laboratoires publics ou privés.

Wind turbine quantification and reduction of uncertainties based on a data-driven data assimilation approach

Adrien Hirvoas,^{1,2} Clémentine Prieur,² Élise Arnaud,² Fabien Caleyron,¹ and Miguel Munoz Zuniga³

¹*IFP Energies nouvelles, Rond-point de l'échangeur de Solaize, BP 3, 69360 Solaize, France*

²*Univ. Grenoble Alpes, CNRS, Inria, Grenoble INP* LJK, 3800 GrenobleFrance*

** Institute of Engineering Univ. Grenoble Alpes*

³*IFP Energies nouvelles, 1 et 4 avenue de Bois-Préau, 92852 Rueil-MalmaisonFrance*

(*Electronic mail: adrien.hirvoas@gmail.com)

(Dated: June 15, 2022)

In this paper, we propose a procedure for quantifying and reducing uncertainties impacting numerical simulations involved in the estimation of the fatigue of a wind turbine structure. The present study generalizes a previous work carried out by the authors proposing to quantify and to reduce uncertainties affecting the properties of a wind turbine model by combining a global sensitivity analysis and a recursive Bayesian filtering approach. We extend the procedure to include the uncertainties involved in the modeling of a synthetic wind field. Unlike the model properties having a static or slow time-variant behavior, the parameters related to the external solicitation have a non-explicit dynamic behavior which must be taken into account during the recursive inference. A non-parametric data-driven approach to approximate the non-explicit dynamic of the inflow related parameters is used. More precisely, we focus on data assimilation methods combining a nearest neighbor or analog sampler with a stochastic filtering method such as the ensemble Kalman filter. The so-called data-driven data assimilation approach is used to recursively reduce the uncertainties that affect the parameters related to both model properties and wind field. For the approximation of the non-explicit dynamic of the wind inflow related parameters, in-situ observations, obtained from a Light Detection And Ranging system and a cup-anemometer device, are used. For the data-assimilation procedure, synthetic data simulated from the aero-servo-elastic numerical model are considered. The next investigations will be to verify the procedure with real in-situ data.

1 I. INTRODUCTION

2 A major challenge in wind energy industry is to propose robust designs withstanding unknown
3 environmental conditions. Design standards (IEC, 2019) are mainly based on dynamic load simu-
4 lations describing the structural behavior of the wind turbine under different wind and operational
5 conditions weighted by their probability of occurrence. Most of the time the number of wind
6 scenarios considered during the conception phase is moderate and far from exploring the set of
7 environmental conditions. Moreover, the dynamic response of the structure and its lifetime can
8 be affected by some uncertainties or evolution in the wind turbine properties. Consequently, the
9 prediction of the operating wind turbine lifetime by taking into account all the inherent uncertainty
10 is crucial. In that context, the quantification and reduction of uncertainties involved in the aero-
11 servo-elastic numerical models play an important role to determine the effective fatigue loads of
12 the turbine.

13 The approach introduced in this paper generalizes the one in Hirvoas *et al.* (2021) by taking
14 into account the uncertainties affecting the parameters related to the wind inflow. It relies on
15 a complete framework including a global sensitivity analysis, an identifiability analysis, and a
16 recursive Bayesian inference approach. First, a surrogate based global sensitivity analysis through
17 the estimation of Sobol' indices allows one to determine the most relevant input parameters in the
18 variability of the fatigue loads of a wind turbine. After assessing the identifiability properties of
19 these influential parameters, a second objective is to reduce their uncertainty by using an ensemble
20 Kalman filter. Data assimilation allows one to gather all the information obtained from real time
21 measurements of the physical system and from the numerical model. The procedure is closely
22 related to the industrial concept of digital twin which consists in combining measurements from
23 the wind turbine with a numerical model to build a digital equivalent of the real-world structure.
24 However, unlike the model properties having a static or slow time-variant behavior, the parameters
25 related to the external conditions have a dynamic that has to be learnt from data.

26 For design certification, offshore wind turbines in pilot farms are more and more monitored
27 thanks to a large number of sensors. In that context, the measured data can be efficiently used
28 in order to learn the non-explicit dynamic behavior of the wind parameters needed for numerical
29 simulation. In the present work, we focus on non-parametric learning strategies. In the litera-
30 ture, several non-parametric methods have been developed such as regression machine learning
31 (Brunton, Proctor, and Kutz, 2016), echo state networks (Pathak *et al.*, 2018) or more recently

32 residual neural networks (Bocquet, Farchi, and Malartic, 2020). Our study investigates an analog
33 forecasting method relying on the principle of the nearest neighbors (Lorenz, 1969). Analogue
34 methods have the advantage of being computationally inexpensive, so that ensemble forecasts,
35 used in data assimilation, are easy to make. The aforementioned non-parametric procedure has
36 been firstly coupled with data assimilation filtering schemes in (Tandeo *et al.*, 2015) and further
37 detailed by Lguensat *et al.* (2017). In the present work, we propose an algorithm, developed in
38 (Hirvoas *et al.*, 2021), interfacing Python library AnDA¹ combining analog forecasting with en-
39 semble data assimilation. The algorithm we propose takes profit of the parallelization capabilities
40 of high performance computing architectures which allows for example to evaluate the real-time
41 damage of an operating wind turbine using a digital twin.

42 The outline of this paper is as follows. Firstly, Section II describes the different uncertainties
43 involved in the framework of this study. In Section III, the theoretical framework of data-driven
44 data assimilation with a specific focus on the ensemble Kalman filtering scheme coupled with the
45 analog forecasting strategy is detailed. Finally, results of an application of this complete procedure
46 of uncertainty quantification and reduction to a reference wind turbine are presented in Section IV.

47 II. CONTEXT

48 A. Uncertainty in wind turbine modeling

49 Before their exploitation, wind turbine rotors are designed thanks to a site classification strat-
50 egy. It relies on design standard classes characterized by the reference turbulence intensity I_{ref} ,
51 defined as the mean turbulence intensity expected at 15 m/s mean wind speed and the reference
52 wind \bar{u}_{ref} , defined as the extreme 10-minute average wind speed with a recurrence period of 50
53 years. In the IEC-61400-1 standard (IEC, 2019), two safety classes are considered. The first one,
54 named as normal safety class, allows one to cover most applications by giving specific values for
55 I_{ref} and \bar{u}_{ref} . In Table I, the corresponding values for the nine categories of the normal safety are
56 given. The proposed parameter values are supposed to represent many different sites and conse-
57 quently do not give a precise representation of a specific site. The second category is mentioned
58 as a special safety class S which allows to consider site-specific values for the wind speed and
59 turbulence terms.

¹ see <https://github.com/ptandeo/AnDA>

Table I. Safety class design classification of the wind turbines: the normal safety class containing nine categories from I-A to III-C and the special safety class S (IEC, 2019) giving the reference turbulence intensity I_{ref} and the reference wind speed \bar{u}_{ref}

Wind turbine Generators class		I	II	III	S	
		\bar{u}_{ref} [m/s]	50	42.5	37.5	Site-specific values
Turbulence class	A	I_{ref} [-]	0.16			
	B		0.14			
	C		0.12			

60

61

62 For each class, the design relies on numerical aero-servo-elastic simulations under different
63 environmental and operational conditions. They allow one to estimate the ultimate and fatigue
64 loads in order to certify the structural integrity. Nevertheless, operating wind turbines experience
65 real wind and operational conditions that can differ from the ones mentioned in the design standard
66 classes. Consequently, there is a need for an estimation of the fatigue life of the structure based on
67 the real wind solicitation seen by the structure. Moreover, the wind turbine itself can present some
68 uncertainties or evolution in its mechanical properties (defaults appearance, degradation with time)
69 that will affect the dynamic response of the structure and its lifetime.

70 As a consequence, these aero-servo-elastic numerical models involve many uncertain and po-
71 tentially variable over time parameters. The ubiquitous uncertainty may be found in the parameters
72 of the wind turbine numerical model as well as in the external conditions. To ensure the track-
73 ing of fatigue and defaults of an operating wind turbine structure, it is important to quantify the
74 impact of these uncertainties on predictions and then to reduce them based on the combination of
75 measurements and model predictions. For that purpose, the field of uncertainty quantification is
76 well-adapted. Hereafter, we propose to determine the sources of uncertainties affecting the wind
77 field parameters and the wind turbine numerical model properties.

78 **1. Uncertainties in wind field modeling**

79 First, the uncertainty of wind field parameters has to be determined. In our context, these
80 parameters are used to characterize a synthetic three-dimensional turbulent wind field based on

81 the Kaimal spectrum (Kaimal *et al.*, 1972) having a one-sided power spectral density defined as:

$$82 \quad S_k(f) = \frac{4\sigma_k^2 \frac{L_k}{u}}{(1 + 6f \frac{L_k}{u})^{\frac{5}{3}}},$$

83 where f is the frequency of occurrence, the subscript $k \in \{u, v, w\}$ represents the turbulent longitu-
 84 dinal, crosswise or vertical components, L_k is the Kaimal length scale, u is the longitudinal mean
 85 wind speed at hub height, and σ_k is the standard deviation of the wind speed.

86 The wind inflow over the swept area is generated based on a grid of points thanks to an ex-
 87 ponential spatial coherence method (Jonkman, 2009). The related coherence function for the lon-
 88 gitudinal wind component of two distinct points i and j separated by a distance Δr on a plan
 89 perpendicular to the wind direction is defined as:

$$90 \quad \text{coh}_{i,j}(f) = \exp \left(-a \left(\frac{\Delta r}{z_m} \right)^\gamma \sqrt{\left(\frac{f \Delta r}{\bar{u}_m} \right)^2 + \left(\frac{b' \Delta r}{L_u} \right)^2} \right), \quad (1)$$

91 where z_m and \bar{u}_m are respectively the mean height of the two points and the mean of the wind speeds
 92 of the two points, a and b' are respectively the input coherence decrement and offset parameter,
 93 and γ is the coherence exponent.

94 Eight input parameters related to the wind field have been identified to be tainted by uncertain-
 95 ties, see Table II. We have considered the mean and the standard deviation of the wind speed at hub
 96 height, the vertical wind shear exponent, the mean wind inflow direction relative to the wind tur-
 97 bine in terms of vertical or horizontal inflow angles, and the longitudinal turbulence length scale
 98 parameter. Moreover, we have supposed as unknown the input coherence decrement and offset
 99 parameter.

100 In an operational context, some information on the mean and standard deviation of the wind
 101 speed at hub height can be obtained from 10-minute data measured from a nacelle mounted
 102 anemometer. Nevertheless, these measurements are known to be very perturbed and never fully
 103 describe the parameters of interest due mainly to the wake effect of the rotor and the non-exact
 104 transfer function used to retrieve them. In this work, we assume that the 10-minute mean and
 105 standard deviation free wind speed can be obtained from the 10-minute data obtained from the
 106 anemometer modulo an additive error term. So that the mean free wind speed at hub height can be

107 obtained from the anemometer as:

$$108 \quad \bar{u} = \bar{u}_{scada} + \Delta\bar{u},$$

109 where \bar{u}_{scada} is the 10-minute mean wind speed obtained from the anemometer mounted on the
110 wind turbine nacelle and $\Delta\bar{u}$ is an additive error assumed to follow the distribution defined in Table
111 II.

112 In a similar manner, the free wind speed standard deviation can be obtained from the measure-
113 ment obtained by the anemometer mounted on the nacelle of the wind turbine as:

$$114 \quad \sigma_u = \sigma_{scada} + \Delta\sigma_u,$$

115 where σ_{scada} is the 10-minute standard deviation wind speed obtained from the nacelle anemome-
116 ter of the wind turbine nacelle and $\Delta\sigma_u$ is an additive error assumed to follow the distribution
117 defined in Table II.

118 Unless having high frequency supervisory control and data acquisition system (SCADA) data,
119 no information can be obtained on the other parameters. An investigation of the distribution of
120 the uncertainty affecting these remaining wind inflow parameters has to be properly made. The
121 vertical wind shear is modeled with the following power law that uses a shear coefficient α :

$$122 \quad \bar{u}_z = \bar{u} \times \left(\frac{z}{z_{hub}} \right)^\alpha,$$

123 where \bar{u} is the prescribed hub-height mean wind velocity, z is the vertical distance from the ground
124 surface, z_{hub} is the hub height, and α is the vertical wind shear coefficient. We adapt the **the mean**
125 **and the standard deviation of the** Gaussian distribution proposed by Dimitrov, Natarajan, and Kelly
126 (2015) for the 10-minute vertical wind shear exponent, such that:

$$127 \quad \begin{aligned} \mu_\alpha &= 0.088(\ln(\bar{u}_{scada}) - 1) \\ \sigma_\alpha &= 1/\bar{u}_{scada} \end{aligned} \quad (2)$$

128 Table II summarizes the wind-inflow parameters that we consider unknown and their respective
129 uncertainty modeling. In particular, we defined the probability distributions of the parameters used
130 in the exponential coherence model defined in Equation (1).

Table II. Wind field parameters - uncertainties affecting the inputs of the wind turbine model. \mathcal{U} : uniform distribution and \mathcal{G} : Gaussian distribution.

Input	Variable	Unit	Distribution	Parameters	REF
Error of hub mean wind speed SCADA vs undisturbed inflow	$\Delta\bar{u}$	[m/s]	\mathcal{U}	Min: $-0.15 \cdot \bar{u}_{scada}$ Max: $0.15 \cdot \bar{u}_{scada}$	Expert knowledge
Error of hub standard deviation SCADA vs undisturbed inflow	$\Delta\sigma_u$	[m/s]	\mathcal{U}	Min: $-0.2 \cdot \sigma_{scada}$ Max: $0.2 \cdot \sigma_{scada}$	Expert knowledge
Vertical wind inflow angle	ϕ_v	[°]	\mathcal{U}	Min: 0 Max: 10	Expert knowledge
Horizontal wind inflow angle	ϕ_h	[°]	\mathcal{U}	Min: -15 Max: 15	Expert knowledge
Longitudinal turbulence length scale	Λ_u	[m]	\mathcal{U}	Min: 20 Max: 170	(Dimitrov, Natarajan, and Mann, 2017) (Solari and Piccardo, 2001)
Decrement parameter of coherence model	a	[-]	\mathcal{U}	Min: 1.5 Max: 26	(Robertson <i>et al.</i> , 2019a)
Offset parameter of coherence model	b'	[-]	\mathcal{U}	Min: 0 Max: 0.17	(Robertson <i>et al.</i> , 2019a) (Saranyasootorn, Manuel, and Veers, 2004)
Vertical wind shear exponent	α	[-]	\mathcal{G}	$\mu = \mu_\alpha$ $\sigma = \sigma_\alpha$, see Equation (2)	(Dimitrov, Natarajan, and Kelly, 2015)

131 2. Uncertainties in aero-servo-elastic numerical model

132 Moreover, as suggested in Hirvoas *et al.* (2021), a total of twelve parameters can be consid-
133 ered as uncertain in the aero-servo-elastic wind turbine numerical model properties. All these
134 input parameters are assumed to be independent of one another with Gaussian or truncated Gaus-
135 sian distributions obtained from expert knowledge or literature. Considering the support structural
136 properties of the turbine model, we have selected six parameters: as nacelle mass and center of
137 mass, tower Rayleigh damping, inertial nacelle and drive-train torsion stiffness. Lastly, the geome-
138 try of the tower, resulting from fabrication tolerances, has been also included in these uncertainties
139 by uniformly scaling the distributed tower thickness. The probability distribution of this last men-
140 tioned parameter is determined by changing the first fore-aft tower frequency mode by $\pm 10\%$ of
141 its nominal value. The uncertainties in blade structural properties have been represented using
142 five parameters. The blade structural responses have led to the definition of the uncertainty range.
143 Indeed, the frequency of the edge-wise (EW) and flap-wise (FW) modes are changed about 10%
144 each from their reference value. These modifications of the frequency modes are done by uni-
145 formly scaling the associated stiffness and the distributed blade mass of all blades. For anomaly
146 diagnosis, blade mass imbalance effects have been also included by applying a different mass fac-
147 tor value to each blade. One blade's mass property is modified to be a value that is higher than the
148 nominal value, and another one modified to a lower value. The third blade remains unchanged at
149 the nominal value. Finally, for the individual blade pitch error, a constant offset angle is applied
150 to two of the blades, respectively above and below the nominal value. These different parameters
151 are considered independent from each other. Table III gathers information about the probability

152 distribution of each of these parameters.

Table III. Model parameters - uncertainties affecting the inputs of the wind turbine model. \mathcal{G} : Gaussian distribution and \mathcal{TG} : Truncated Gaussian distribution where a and b are the cut-off parameters.

Input	Variable	Unit	Distribution	Parameters	REF
Nacelle mass	N_{mass}	[kg]	\mathcal{G}	$\mu = 6.90e+04$ $\sigma = 2.30e+03$	(Witcher, 2017)
Nacelle center of mass	N_{CMx}	[m]	\mathcal{G}	$\mu = 1.00$ $\sigma = 3.35e-02$	(Robertson <i>et al.</i> , 2019b)
Tower thickness adding coefficient	e	[-]	\mathcal{G}	$\mu = 0.00$ $7.00e-01$	Expert knowledge $\pm 10\%$ 1 FA
Tower Rayleigh damping	β_{TR}	[-]	\mathcal{TG}	$\mu = 2.55$ $\sigma = 0.82$ $a = \mu - 3\sigma$ $b = \mu + 3\sigma$	(Koukoura, 2014)
Inertial nacelle	I_{zz}	[kg · m ²]	\mathcal{G}	$\mu = 7.00e+05$ $\sigma = 2.33e+04$	Expert knowledge $\pm 10\%$ μ
Drive-train torsional stiffness	K_D	[$\frac{N \cdot m^2}{rad}$]	\mathcal{G}	$\mu = 9.08e+09$ $\sigma = 3.03e+07$	(Holierhoek <i>et al.</i> , 2010)
Blade flap wise stiffness	α_{BF}	[N · m ²]	\mathcal{G}	$\mu = 1.00$ $\sigma = 3.33e-02$	Expert knowledge $\sim \pm 10\%$ 1 FW
Blade edge wise stiffness	α_{BE}	[N · m ²]	\mathcal{G}	$\mu = 1.00$ $\sigma = 3.33e-02$	Expert knowledge $\sim \pm 10\%$ 1 EW
Blade mass coefficient	α_{mass}	[-]	\mathcal{G}	$\mu = 1.00$ $\sigma = 1.67e-02$	(Witcher, 2017)
Blade Rayleigh damping	β_{BR}	[-]	\mathcal{TG}	$\mu = 1.55$ $\sigma = 4.83e-01$ $a = \mu - 3\sigma$ $b = \mu + 3\sigma$	(Robertson <i>et al.</i> , 2019b)
Blade mass imbalance	η_B	[-]	\mathcal{G}	$\mu = 2.50e-02$ $\sigma = 8.33e-03$	(Robertson <i>et al.</i> , 2019b)
Individual pitch error	Ω	[°]	\mathcal{G}	$\mu = 0.10$ $\sigma = 3.33e-02$	(Simms <i>et al.</i> , 2001)

153

154

155 B. Methodology for uncertainty quantification

156 In the monitoring context of an operating wind turbine, one of the major challenges is to predict
 157 the remaining lifetime of the structure. Hence, the current study focuses on a complete framework
 158 first quantifying and then reducing in a recursive fashion the uncertainties affecting the damage
 159 loads obtained from an aero-servo-elastic simulation. Hereafter, we will focus on the estimation
 160 of the effective damage equivalent load (DEL) describing the fatigue behavior of the wind turbine
 161 at some specific locations. The DEL is obtained by considering the internal loads and is defined
 162 as a virtual load amplitude that would create, in reference regular cycles, the same damage as the
 163 considered irregular load history.

164 The aim of the work in this article is to generalize the complete methodology proposed in
 165 (Hirvoas *et al.*, 2021) for quantifying and reducing the uncertainties affecting a wind turbine nu-
 166 merical model by handling wind turbine model properties in addition to wind inflow uncertainties,

167 respectively denoted by \mathbf{x}^1 and \mathbf{x}^2 in Figure 1.

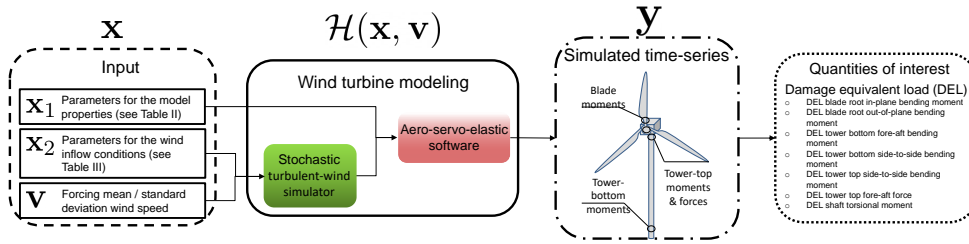


Figure 1. Wind turbine modeling framework, where \mathbf{x} is the extended vector gathering both uncertainties from wind inflow parameters and model properties.

168 The procedure relies on a global sensitivity analysis (GSA) based on Sobol' index estimation
 169 and a recursive Bayesian inference procedure to reduce the uncertainties, similarly as in (Hirvoas
 170 *et al.*, 2021). In order to alleviate the computational cost of index estimation during the sensitivity
 171 analysis of the fatigue loads, the aero-servo-elastic time-consuming numerical model is approxi-
 172 mated by a surrogate. A major challenge in building such surrogate model relies on the fact that
 173 the turbulent wind inflow realization causes variations in the quantities of interest obtained from
 174 the model. Thus, to take into account the inherent variability on the turbine response induced
 175 by different turbulent wind field realizations, the approach focuses on the use of heteroscedastic
 176 Gaussian process regression models. Then, a recursive reduction of the influent parameter uncer-
 177 tainties based on an ensemble Kalman filter is proposed. This data assimilation filtering method is
 178 computationally efficient with high-performance computing tools which is a major advantage for
 179 online calibration of time-consuming codes, such as aero-servo-elastic wind turbine models. Nev-
 180 ertheless, a challenge in this kind of inverse problem is to determine whether the measurements are
 181 sufficient to unambiguously determine the parameters that generated the observations, i.e., iden-
 182 tifiability properties. In that context, GSA is also proposed to detect non identifiable parameters
 183 considering the current measurements.

184 The main contribution of the presented work is the inference of parameters involved in both
 185 the model properties of the wind turbine having a static or slow evolution and the short-term wind
 186 inflow varying at each inference iteration of 10-minute. To take into account the non-explicit
 187 dynamics of the parameters related to the wind inflow in the recursive inference procedure, the
 188 study relies on a data-driven approach combining a K -nearest neighbors with an ensemble Kalman
 189 filtering scheme. In the next section, we propose to describe this data-driven procedure used in our
 190 model calibration strategy.

191 III. DATA-DRIVEN DATA ASSIMILATION

192 A. Data assimilation

193 State-space model (SSM) is a useful framework to perform recursive inference strategy such as
 194 sequential data assimilation techniques (Bertino, Evensen, and Wackernagel, 2003; Durbin and
 195 Koopman, 2012; Hirvoas *et al.*, 2021). In order to take into account the information obtained
 196 from the SCADA system of the wind turbine, we consider the SSM formulation involving forcing
 197 variables defined $\forall k \in \mathbb{N}^*$ as:

$$\mathbf{x}_{(k)} = \mathcal{M}_{(k-1,k)}(\mathbf{x}_{(k-1)}) + \boldsymbol{\varepsilon}_{(k)}^m, \quad (3)$$

$$\mathbf{y}_{(k)} = \mathcal{H}_{(k)}(\mathbf{x}_{(k)}, \mathbf{v}_{(k)}) + \boldsymbol{\varepsilon}_{(k)}^o. \quad (4)$$

198 where $\mathbf{y}_{(k)}$ corresponds to the observation at step k and $\mathbf{x}_{(k)}$ is a p -dimensional vector representing
 199 the hidden-state variables which depict the input parameters in the aero-servo-elastic numerical
 200 model such that:

$$201 \quad x = \begin{pmatrix} x^1 \\ x^2 \end{pmatrix}$$

202 with $\mathbf{x}_{(k-1)}^1$ and $\mathbf{x}_{(k-1)}^2$ respectively the uncertain parameters for the wind inflow conditions, de-
 203 scribed in Table II, and the model properties, described in Table III. The model denoted by \mathcal{M}
 204 (potentially nonlinear) allows us to describe the dynamic behavior of the hidden process. The
 205 model error $\boldsymbol{\varepsilon}_{(k)}^m$ is supposed to be a Gaussian white noise of zero mean and of covariance $\mathbf{Q}_{(k)}$,
 206 modeling the uncertainties related to the dynamics model structure. The propagator \mathcal{H} relates the
 207 hidden-state vector to the measured observations and contains some forcing variables $\mathbf{v}_{(k)}$, e.g.,
 208 mean wind speed obtained from the anemometer of the wind turbine. The sources of errors in the
 209 observation model defined in Equation (4) are reflected by the Gaussian white noise of zero mean
 210 and of covariance $\mathbf{R}_{(k)}$, denoted by $\boldsymbol{\varepsilon}_{(k)}^o$, and assumed to be independent of the model error $\boldsymbol{\varepsilon}_{(k)}^m$.
 211 This SSM formulation can be represented thanks to the directed graph given below.

$$\begin{array}{ccccccc}
212 & & & (\mathcal{M}_{(k-1,k)}, \mathbf{Q}_{(k)}) & & & \\
\text{Hidden-state} & \cdots \rightarrow & \mathbf{x}_{(k-1)} & \rightarrow & \mathbf{x}_{(k)} & \rightarrow & \mathbf{x}_{(k+1)} \rightarrow \cdots \\
& & \downarrow & & \downarrow & (\mathcal{H}_{(k)}, \mathbf{v}_{(k)}, \mathbf{R}_{(k)}) & \downarrow \\
\text{Observations} & & \mathbf{y}_{(k-1)} & & \mathbf{y}_{(k)} & & \mathbf{y}_{(k+1)}
\end{array}$$

213 B. Data-driven data assimilation

214 In many situations, the dynamical model \mathcal{M} is numerically intractable or unknown. In the
215 literature different studies have been conducted to emulate this propagator, used in Equation (3),
216 from historical data. Several surrogate techniques have been employed for the reconstruction of
217 nonlinear dynamics model of chaotic system. Authors in (Tandeo *et al.*, 2015) propose a K -nearest
218 neighbors based method, also known as the analog strategy in meteorology or geoscience com-
219 munity. Nevertheless, it has been argued that methods relying on a K -nearest neighbors technique
220 are plagued by the curse-of-dimensionality, i.e., fails in very high dimensional applications (Fried-
221 man, 1997; Chen, 2009). Consequently, other non-parametric surrogate modeling approaches
222 have been investigated to learn the underlying dynamics by using for example regression machine
223 learning (Brunton, Proctor, and Kutz, 2016), echo state networks (Pathak *et al.*, 2018) or more
224 recently residual neural networks (Bocquet, Farchi, and Malartic, 2020).

225 Due to the limited dimension of our inference problem, we have decided to investigate and
226 to use the analog forecasting strategy coupled with data assimilation proposed in (Tandeo *et al.*,
227 2015; Hamilton, Berry, and Sauer, 2016; Lguensat *et al.*, 2017). Analog forecasting is related
228 to the notion of atmospheric predictability introduced by Lorenz (1969). Later, this approach has
229 been widely used in several atmospheric, oceanic, and climate studies (Toth, 1989; Alexander
230 *et al.*, 2017; Ayet and Tandeo, 2018). Hereafter, we detail the principle of the analog forecasting
231 technique.

232 The main idea of the methodology is to substitute the dynamical model in Equation (3) by a
233 data-driven model relying on an analog forecasting operator, denoted by \mathcal{A} , such as :

$$234 \forall k \in \mathbb{N}^*, \begin{cases} \mathbf{x}_{(k)} = \mathcal{A}_{(k-1,k)}(\mathbf{x}_{(k-1)}) + \boldsymbol{\varepsilon}_{(k)}^m \\ \mathbf{y}_{(k)} = \mathcal{H}_{(k)}(\mathbf{x}_{(k)}, \mathbf{v}_{(k)}) + \boldsymbol{\varepsilon}_{(k)}^o \end{cases} .$$

235 The analog forecasting principle consists in searching for one or several similar situations of the
 236 current hidden-state vector that occurred in historical trajectories of the system of interest, then
 237 retrieving the corresponding successors of these situations, and finally assume that the forecast
 238 of the hidden-state can be retrieved from these successors. Consequently, this strategy requires
 239 the existence of a representative catalog of historical data, denoted by \mathcal{C} . The reference catalog is
 240 formed by pairs of consecutive hidden-state vectors, separated by the same lag (Fablet *et al.*, 2017).
 241 The first component of each pair is named as the analog (denoted by \mathbf{a}) while the corresponding
 242 state is referred to as the successor (noted as \mathbf{s}). The corresponding representative dataset of
 243 hidden-state sequences can be written as:

$$244 \quad \mathcal{C} = \{(\mathbf{a}_i, \mathbf{s}_i), i = [1 \cdots P]\}, \text{ with } P \in \mathbb{N}^*.$$

245 This historical catalog can be constructed using observational data recorded using in-situ sensors as
 246 well as from numerical simulations. Based on this database, the analog forecasting operator \mathcal{A} is
 247 a non-parametric data-driven sampling of the state from iteration $k - 1$ to iteration k . Three analog
 248 forecasting operators have been originally proposed by the authors in Lguensat *et al.* (2017). They
 249 are all based on nearest neighbors of the hidden-state in the reference catalog \mathcal{C} weighted thanks
 250 to a kernel function. Among the different kernels, Chau, Ailliot, and Monbet (2021) propose to
 251 use a tricube kernel which has a compact support and is smooth at its boundary. Throughout this
 252 article, as selected by Lguensat *et al.* (2017), a radial basis function (also known as Gaussian
 253 kernel, squared exponential kernel, or exponentiated quadratic) is considered and defined as:

$$254 \quad g(\mathbf{u}, \mathbf{v}) = \exp\left(-\lambda \|\mathbf{u} - \mathbf{v}\|^2\right), \quad (5)$$

255 where (\mathbf{u}, \mathbf{v}) are two distinct variables in the hidden-state space, λ is a scale parameter, and $\|\cdot\|$
 256 is the Euclidean distance or any other relevant distance function for our application. The kernel
 257 choice is case dependent. The Gaussian kernel used hereafter is isotropic and parameterized by λ
 258 allowing to easily control the bandwidth.

259 Let us denote by $\{\mathbf{a}_n\}_{n \in \mathcal{I}}$ the K -nearest neighbors (also known as analog situations) of a given
 260 hidden-state at iteration $k - 1$, where $\mathcal{I} = \{i_1, \dots, i_K\}$ contains the K indices of these situations.
 261 From the reference catalog \mathcal{C} , one can retrieve the corresponding successors $\{\mathbf{s}_n\}_{n \in \mathcal{I}}$. Then
 262 for every pair of analog and successor $(\mathbf{a}_n, \mathbf{s}_n)_{n \in \mathcal{I}}$, a normalized kernel weight $(\omega_n)_{n \in \mathcal{I}}$ can be

263 assigned such that:

$$264 \quad \omega_n = \frac{g(\mathbf{x}_{(k-1)}, \mathbf{a}_n)}{\sum_{j=1}^K g(\mathbf{x}_{(k-1)}, \mathbf{a}_{i_j})}.$$

265 This term provides more importance to pairs that are best suited according to the kernel function
266 for the estimation of the hidden-state $\mathbf{x}_{(k)}$ in the K -nearest neighbors obtained from the catalog.
267 Nevertheless, the parametrization of this weight is highly dependent on the kernel function. More-
268 over in the context of the Gaussian kernel as defined in Equation (5), the normalized kernel weight
269 involves the choice of the number of nearest neighbors K and the scale parameter λ . Two common
270 strategies in the statistic field are used for the estimation of K : either a distance threshold in order
271 to consider the nearest neighbors which respect it, or an expert based number of analogs (Peterson,
272 2009). In our work, we consider the last strategy for simplicity. As proposed by Lguensat *et al.*
273 (2017), the scale parameter can be fixed following the adaptive rule defined as:

$$274 \quad \lambda = \frac{1}{\text{md}(\mathbf{x}_{(k-1)})},$$

275 where $\text{md}(\mathbf{x}_{(k-1)})$ is the median distance between the hidden-state at iteration $k - 1$ and its K
276 nearest neighbors. Nevertheless, a more sophisticated procedure not used hereafter, based on a
277 cross-validation procedure, can be employed to optimize the choice of these hyper-parameters.

278 Three analog forecasting operators \mathcal{A} have been defined in (Lguensat *et al.*, 2017). The com-
279 plexity of model studied and the available computational resources are the two main constraints
280 that will drive the choice of one forecasting operator over the others. For example in situations
281 facing some extreme values of the hidden-state based on the available catalog, the locally-constant
282 gives poor results due to the fact that the forecasting estimate is held in the range of K -nearest
283 neighbors. In that context, the locally-incremental and the locally-linear forecasting operators are
284 much more efficient (Lguensat *et al.*, 2017). A graphical representation of the three different ana-
285 log forecasting operators for a 2-dimensional hidden-state is given in Figure 2. In this example, the
286 underlying dynamics model has a simple polynomial form and the analogs are obtained by using
287 a normal distribution sampling centered on the real value of the hidden-state at iteration $k - 1$. [In](#)
288 [this research work, we have decided to focus on the locally-linear operator.](#)

289 The locally-linear forecasting operator consists of performing a weighted least square linear
290 regression between the K -nearest neighbors and their corresponding successors in the catalog \mathcal{C} .
291 The multivariate linear regression provides a slope matrix of size $p \times p$ denoted by α , a vector

292 intercept of size $p \times 1$ designated hereafter by β , and residuals defined as the following vectors
 293 $\forall j \in [1, \dots, K], \mathbf{s}_{ij} - (\alpha \mathbf{a}_{ij} + \beta)$. The Gaussian sampling resorts to:

294
$$\mathbf{x}_{(k)}^f \sim \mathcal{N}(\boldsymbol{\mu}_{(k)}^{\text{LL}}, \boldsymbol{\Sigma}_{(k)}^{\text{LL}}),$$

295 where the mean forecast is $\boldsymbol{\mu}_{(k)}^{\text{LL}} = \alpha \mathbf{x}_{(k-1)} + \beta$, and $\boldsymbol{\Sigma}_{(k)}^{\text{LL}}$ is the weighted empirical covariance of
 296 the residuals thanks to the normalized kernel weight $(\omega_n)_{n \in \mathcal{I}}$.

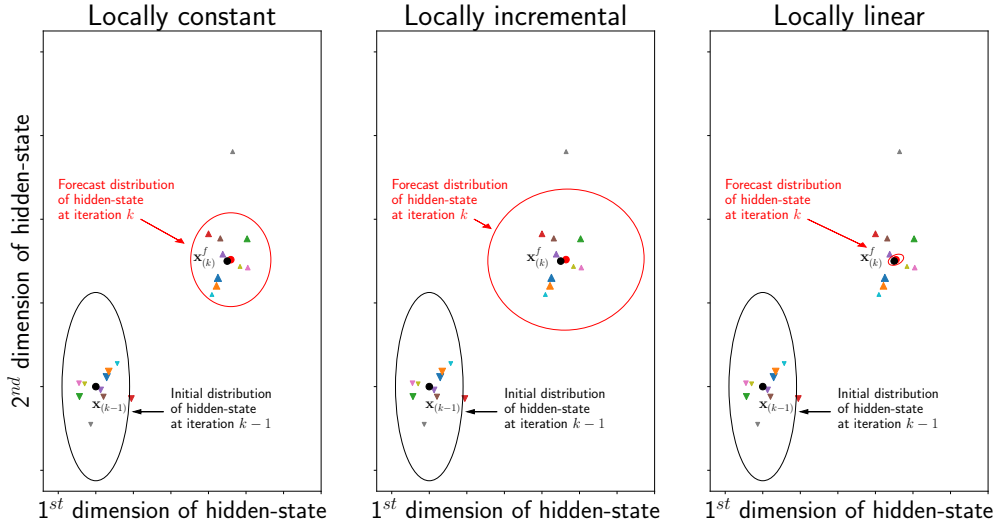


Figure 2. Analog forecasting operator strategies. The hidden-state real values $\mathbf{x}_{(k-1)}$ and its forecast $\mathbf{x}_{(k)}$ are represented by full circles. Analogs are displayed in colored down-pointing triangles and successors in up-pointing triangles with their equivalent colors. Each triangle size is proportional to the normalized kernel weight. The ellipsoids in black and red represent respectively the 95 % confidence intervals of the hidden state distribution before and after the analog forecasting strategy.

297 **C. Non-parametric EnKF method**

298 Hereafter, we propose to describe the data assimilation framework coupled with the analog
 299 forecasting method firstly proposed by Tandeo *et al.* (2014) and further detailed in (Lguensat
 300 *et al.*, 2017). Data assimilation methods allow us to combine all the sources of information ob-
 301 tained from a physical model and observations. In particular, sequential data assimilation tech-
 302 niques, also known as filtering approaches consist of estimating the filtering posterior distribution
 303 of the current hidden-state knowing past and present observations $p_{\mathbf{X}_{(k)}|\mathbf{Y}_{(1:k)}}(\mathbf{x}_{(k)}|\mathbf{Y}_{(1:k)})$ where
 304 $\mathbf{Y}_{(1:k)} = [\mathbf{Y}_{(1)}, \dots, \mathbf{Y}_{(k)}]$. Different methods are available in order to compute the filtering distribu-
 305 tion of interest. In the context of linear Gaussian state-space models, Kalman filter methods can

306 be considered to provide the exact filtering methods (Kalman, 1960; Brown, 1986; Harvey, 1990;
 307 Haykin, 2004; Wells, 2013). Nevertheless in real applications, the linear assumption is often un-
 308 realistic and more sophisticated Kalman-based approaches have to be used (Julier and Uhlmann,
 309 1997; Evensen, 2009). In particular, the ensemble Kalman filter (EnKF) which is a Monte Carlo
 310 variant relying on an ensemble of members to represent the statistics. This sequential Monte Carlo
 311 filter, introduced by Evensen (1994), is widely used in data assimilation applications to take into
 312 account the nonlinearities in the state-space formulation and to handle the high dimensional prob-
 313 lems (Houtekamer and Mitchell, 2001; Snyder and Zhang, 2003; Aanonsen *et al.*, 2009). The
 314 principle of the EnKF is to sequentially update all members of the ensemble by means of a cor-
 315 rection term relying on the Kalman gain which allows **one** to blend the model responses and the
 316 observations at a given iteration, see **Evensen (2003)**. Due to the fact that this approach is based on
 317 an ensemble, it is inherently well-adapted to parallelization which is a crucial advantage with the
 318 current high-performance computing architectures for the inference of time-consuming numerical
 319 models (Houtekamer, He, and Mitchell, 2014).

320 Thus, we present the formulation of a non-parametric EnKF method, also known as analog
 321 EnKF (AnEnKF), see (Tandeo *et al.*, 2014; Lguensat *et al.*, 2017). The procedure is similar to
 322 the stochastic ensemble Kalman recursion (Evensen, 2009). Nevertheless, the main difference of
 323 the AnEnKF occurs for the forecast step where the non-parametric data-driven sampling, i.e., the
 324 analog forecasting operator, is used instead of the dynamic model \mathcal{M} in Equation (3). The analog
 325 ensemble Kalman filter **applies** one of the three analog forecast sampling strategies, presented in
 326 (Lguensat *et al.*, 2017), to each analysis member of the ensemble to generate a forecast term **at each**
 327 **iteration**. Then, the equations used in the procedure are equivalent to the EnKF strategy. At each
 328 iteration during the analysis step, each forecast member of the ensemble is corrected by computing
 329 $\mathbf{x}_{(k)}^{a(i)} = \mathbf{x}_{(k)}^{f(i)} + \mathbf{K}_{(k)} \left(\mathbf{y}_{(k)}^{(i)} - \mathcal{H}_{(k)}(\mathbf{x}_{(k)}^{f(i)}, \mathbf{v}_{(k)}) \right)$ where $\mathbf{K}_{(k)} = \mathbf{P}_{(k)}^f \mathbf{H}_{(k)}^T \left(\mathbf{R}_{(k)} + \mathbf{H}_{(k)} \mathbf{P}_{(k)}^f \mathbf{H}_{(k)}^T \right)^{-1}$ is
 330 named as the Kalman Gain with $\mathbf{P}_{(k)}^f$ the forecast covariance matrix and $\mathbf{H}_{(k)}$ the observation
 331 operator. Due to the nonlinearity of the model $\mathcal{H}_{(k)}$, the terms $\mathbf{P}_{(k)}^f \mathbf{H}_{(k)}^T$ and $\mathbf{H}_{(k)} \mathbf{P}_{(k)}^f \mathbf{H}_{(k)}^T$ are
 332 respectively empirically estimated based on the ensemble members. The ensemble Kalman filter
 333 coupled with the analog forecasting strategy is detailed in Algorithm 1.

Algorithm 1 Ensemble Kalman Filter with analog forecast methodology, so-called AnEnKF.

- 1: Input:
- 2: number of members in the ensemble N_{ens} ;
- 3: number of inference iterations T ;
- 4: catalog \mathcal{C} and number of nearest neighbors K ;
- 5: prior guess of the parameter vector \mathbf{x}_b and prior parameter covariance matrix \mathbf{P}_b .
- 6: Initialisation step:
- 7: **for** $i = 1$ to N_{ens} **do**
- 8: $\mathbf{x}_{(0)}^{a(i)} = \mathbf{x}_b + \boldsymbol{\varepsilon}^b$ with, $\boldsymbol{\varepsilon}^b \sim \mathcal{N}(0, \mathbf{P}_b)$
- 9: **for** $k = 1$ to T **do**
- 10: **Forecast step:**
- 11: **for** $i = 1$ to N_{ens} **do**
- 12: $\mathbf{x}_{(k)}^{f(i)} = \mathcal{A}_{(k-1,k)}(\mathbf{x}_{(k-1)}^{f(i)}) + \boldsymbol{\varepsilon}_{(k)}^{m(i)}$, where,

$$\begin{aligned} \text{Locally-linear analog operator: } \mathcal{A}_{(k-1,k)}(\mathbf{x}_{(k-1)}^{f(i)}) &:= \boldsymbol{\mu}_{(k)}^{LL} = \alpha \mathbf{x}_{(k-1)} + \beta \\ \text{and } \boldsymbol{\varepsilon}_{(k)}^{m(i)} &\sim \boldsymbol{\Sigma}_{(k)}^{LL} \end{aligned}$$

where $(\mathbf{a}_n, \mathbf{s}_n)_{n \in \mathcal{S}}$ (with $\mathcal{S} = \{i_1, \dots, i_K\}$) are the K -pairs of analog and successor for the i -th analysis member of the ensemble at iteration $k-1$ and cov_ω is the weighted covariance.

- 13: **Update step:**

$$\begin{aligned} \mathbf{P}_{(k)}^f \mathbf{H}_{(k)}^T &= \frac{1}{N_{ens} - 1} \sum_{i=1}^{N_{ens}} \left(\mathbf{x}_{(k)}^{f(i)} - \bar{\mathbf{x}}_{(k)}^f \right) \left(\mathcal{H}_{(k)}(\mathbf{x}_{(k)}^{f(i)}, \mathbf{v}_{(k)}) - \mathcal{H}_{(k)}(\bar{\mathbf{x}}_{(k)}^f, \mathbf{v}_{(k)}) \right)^T \\ \mathbf{H}_{(k)} \mathbf{P}_{(k)}^f \mathbf{H}_{(k)}^T &= \frac{1}{N_{ens} - 1} \sum_{i=1}^{N_{ens}} \left(\mathcal{H}_{(k)}(\mathbf{x}_{(k)}^{f(i)}, \mathbf{v}_{(k)}) - \mathcal{H}_{(k)}(\bar{\mathbf{x}}_{(k)}^f, \mathbf{v}_{(k)}) \right) \\ &\quad \left(\mathcal{H}_{(k)}(\mathbf{x}_{(k)}^{f(i)}, \mathbf{v}_{(k)}) - \mathcal{H}_{(k)}(\bar{\mathbf{x}}_{(k)}^f, \mathbf{v}_{(k)}) \right)^T \\ \mathbf{K}_{(k)} &= \mathbf{P}_{(k)}^f \mathbf{H}_{(k)}^T \left(\mathbf{R}_{(k)} + \mathbf{H}_{(k)} \mathbf{P}_{(k)}^f \mathbf{H}_{(k)}^T \right)^{-1} \end{aligned}$$

with $\bar{\mathbf{x}}_{(k)}^f$ the mean of the forecast members of the ensemble

- 14: **for** $i = 1$ to N_{ens} **do**
 - 15: $\mathbf{y}_{(k)}^{(i)} = \mathbf{y}_{(k)} + \mathbf{e}_{(k)}^{o(i)}$ with, $\mathbf{e}_{(k)}^{o(i)} \sim \mathcal{N}(0, \mathbf{R}_{(k)})$
 - 15: $\mathbf{x}_{(k)}^{a(i)} = \mathbf{x}_{(k)}^{f(i)} + \mathbf{K}_{(k)} \left(\mathbf{y}_{(k)}^{(i)} - \mathcal{H}_{(k)}(\mathbf{x}_{(k)}^{f(i)}, \mathbf{v}_{(k)}) \right)$
-

334 IV. NUMERICAL RESULTS

335 In this section, the numerical results of the proposed methodology to quantify and reduce the
336 uncertainties based on global sensitivity analysis and a data-driven data assimilation approach are
337 presented in the context of an industrial operating wind turbine. The two categories of param-

338 eters investigated in this application are the wind turbine model properties and the wind-inflow
 339 conditions. In the sensitivity analysis of the fatigue loads of the wind turbine, we assume that
 340 the 10-minute mean and standard deviation obtained from the SCADA are respectively equal to
 341 10 m/s and 1.4 m/s .

342 A. Case description

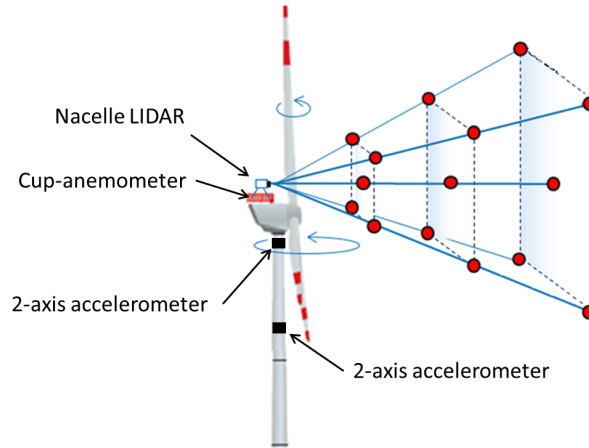
343 For the purpose of this work, the considered model is a numerical representation of a reference
 344 2MW onshore horizontal-axis wind turbine based on the open-source aero-servo-elastic software
 345 FAST developed by the National Renewable Energy Laboratory (NREL) (Jonkman, Buhl Jr. *et al.*,
 346 2005). This numerical code employs a combined modal and multibody dynamics formulation
 347 which allows one to consider a limited degree of freedom number for the structure. Moreover, the
 348 aerodynamic model relies on the blade-element momentum theory coupled with some corrections,
 349 e.g., dynamic stall. The generation of the synthetic turbulent wind field solicitation uses a Kaimal
 350 turbulence model with an exponential spatial coherence method thanks to the TurbSim software
 351 (Jonkman, 2009). Some specifications of the turbine are presented in Table IV.

Table IV. Reference wind turbine specifications.

Quantity	Value
Number of blades	3
Rated power	2.0 MW
Rotor speed range	8.5 – 17.1 rpm ($\pm 16\%$)
Rated wind speed	13 m/s
Cut-in wind speed	3.0 m/s
Cut-out wind speed	25 m/s
Rotor radius	41 m
Hub height	80 m

352 The in situ data used to assess the performances of our procedure are based on a specific mea-
 353 surement campaign of eight months from the French national project SMARTEOLE. For that pur-
 354 pose, the wind turbine has a SCADA gathering 10-minute statistics about the external conditions
 355 at the level of the nacelle hub, e.g., wind speed or direction, and also information on the turbine
 356 operation, e.g., generator speed, generated power. Alongside, a Light Detection And Ranging (LI-
 357 DAR) system is placed on top of the wind turbine nacelle in order to measure the upstream wind
 358 flow conditions. A graphical representation of the monitoring system configuration is proposed

359 in Figure 3. In the study, we suppose that the wind speed at hub height reconstructed from the
 360 LIDAR system is the free wind to be applied on the servo-aero-elastic model through the synthetic
 361 turbulence wind field. Lastly, bi-axial measuring devices are located at mid and top tower height
 362 position. From these sensors, we can record four functional acceleration time series. Then, the
 363 power spectral density (PSD) of each measured acceleration time series is computed using Welch's
 364 method (Welch, 1967).



365 Figure 3. Monitoring system configuration for the reference wind turbine.
 366

367 B. Global sensitivity analysis on fatigue loads

368 To quantify the importance of each input parameter on the variability of the fatigue loads ob-
 369 tained from the aero-servo-elastic numerical model, a global sensitivity analysis (GSA) based on
 370 Sobol' index estimation has been investigated. We focus our interest on total Sobol' sensitivity
 371 indices (Sobol', 1990). The total Sobol' index associated with each input parameter represents the
 372 amount of variance due to the quantity of interest alone or in interaction with any other subset of
 373 parameters. It allows one to quantify the part of variation in the damage equivalent load that could
 374 be reduced if the parameter was to be fixed to a single value. To alleviate the computational cost
 375 in the sensitivity index estimation, heteroscedastic Gaussian process (GP) models (Ginsbourger
 376 *et al.*, 2008) are built independently for each Damage Equivalent Load (DEL). The notion of dam-
 377 age equivalent load (DEL) (Veldkamp, 2006) is often used and is defined as a virtual stress ampli-
 378 tude that would create the same fatigue damage as a particular load history considering a specific
 379 number of regular cycles. These short-term fatigue estimations are computed from the load time

380 series, obtained from the aero-servo-elastic model, by applying a rain-flow counting algorithm
381 and the Palmgren-Miner rule for linear fatigue damage accumulation (Hansen, 2015). Fitting such
382 surrogate model to the load behavior of a wind turbine requires a design of experiments covering
383 the range of variation in all parameters. In that context, we rely on a Latin Hypercube Sampling
384 (LHS) with a geometrical criterion maximizing the minimum distance between the design points
385 (i.e., the sample points obtained from the LHS) (Damblin, Couplet, and Iooss, 2013). To testify
386 the accuracy of the fitted surrogate model for each output of interest described in Table V, an
387 augmented LHS of size 200 has been generated. Then, ten different turbulent inflow realizations
388 are generated using the Kaimal spectrum with an exponential spatial coherence model for each
389 point of the DOE, from which the empirical mean and standard deviation of the fatigue loads are
390 estimated. The heteroscedastic property of the GP, as described in (Hirvoas *et al.*, 2021), allows
391 one to capture the global fatigue behavior of the turbine but also to estimate the inherent variabil-
392 ity due to different turbulent wind field realizations. This study leads to a total number of 11,960
393 aero-servo-elastic numerical model evaluations.

394 Eight different model quantities of interest are considered for describing the fatigue behavior of
395 the wind turbine, see Table V. For each output, the total effect Sobol indices are estimated using the
396 corresponding heteroscedastic Gaussian process metamodel based on the estimator proposed by
397 Jansen (1999) and implemented in the function `sobolGP` of the R package `sensitivity` (Iooss *et al.*,
398 2019). The prediction performance of each Gaussian process is quantified thanks to a validation
399 set, not seen during the training phase, and the predictivity coefficient Q^2 (Marrel *et al.*, 2008).
400 In the presented application, the surrogate model have Q^2 factors over at least 0.8. The GSA
401 estimation approach relies on the complete conditional predictive distribution of the metamodel
402 which allows one to evaluate the uncertainty in the estimation due to the Monte Carlo procedure
403 and the surrogate approximation, see (Hirvoas *et al.*, 2021).

Table V. Wind turbine model fatigue load outputs with their Wöhler exponent m (Meyers and Chawla, 2008).

Quantity of interest	m
DEL blade root in-plane bending moment	10
DEL blade root out-of-plane bending moment	10
DEL tower bottom fore-aft bending moment	3
DEL tower bottom side-to-side bending moment	3
DEL tower top side-to-side bending moment	3
DEL tower top fore-aft force	3
DEL shaft torsional moment	3

405 For the estimation procedure, two distinct LHSs with a maximin criterion have been generated.
406 The uncertainty related to the kriging approximation is quantified by using 100 samples from the
407 conditional distribution of the predictor based on the learning sample. Moreover, the uncertainty
408 due to Monte Carlo integration was estimated with a bootstrap procedure with a sample size of
409 100, see Efron (1981) for further details in bootstrapping strategy. The estimated total Sobol'
410 indices for the considered quantities of interest with their corresponding 95% confidence intervals
411 are presented in Figure 4. Most of the outputs have a large total Sobol' index for the errors relative
412 to the wind speed $\Delta\bar{u}$ and $\Delta\sigma_u$. These input parameters have an important impact on the variability
413 of fatigue loads obtained from our aero-servo-elastic numerical model. The vertical wind shear
414 coefficient α has also a clear impact in particular for the torsional moment of the shaft and the
415 out-of-plane bending moment of the blade. The noticeable effect of the wind shear for rotating
416 components can be explained by the fact that they will face cyclic changes in wind velocity if
417 wind shear is considered. Eight other parameters describing the wind inflow conditions or the
418 wind turbine model properties have total Sobol' indices higher to the arbitrary threshold (set to
419 $5.0e - 02$) and can be considered as influential. The arbitrary threshold is used to discriminate
420 efficiently sensitive and insensitive input parameters. For clarity, these parameters are underlined
421 in Figure 4. In particular, we can notice that model property parameters related to tower thickness,
422 lineic mass and mass imbalance related to the blades (e , α_{mass} , and η_B) have a non-negligible
423 influence on fatigue load variance of the considered wind turbine components. The remaining
424 parameters can be fixed to any specific value in their range of variability without affecting the
425 considered fatigue loads. In our research work, these parameters having a negligible influence on
426 fatigue loads are fixed to the mean of their statistical distribution, see Table II and Table III.

427 After assessing the sensitivity analysis of the fatigue load of some critical components of the

428 wind turbine structure, one major challenge is to reduce the uncertainties affecting the most influ-
 429 ential input parameters.

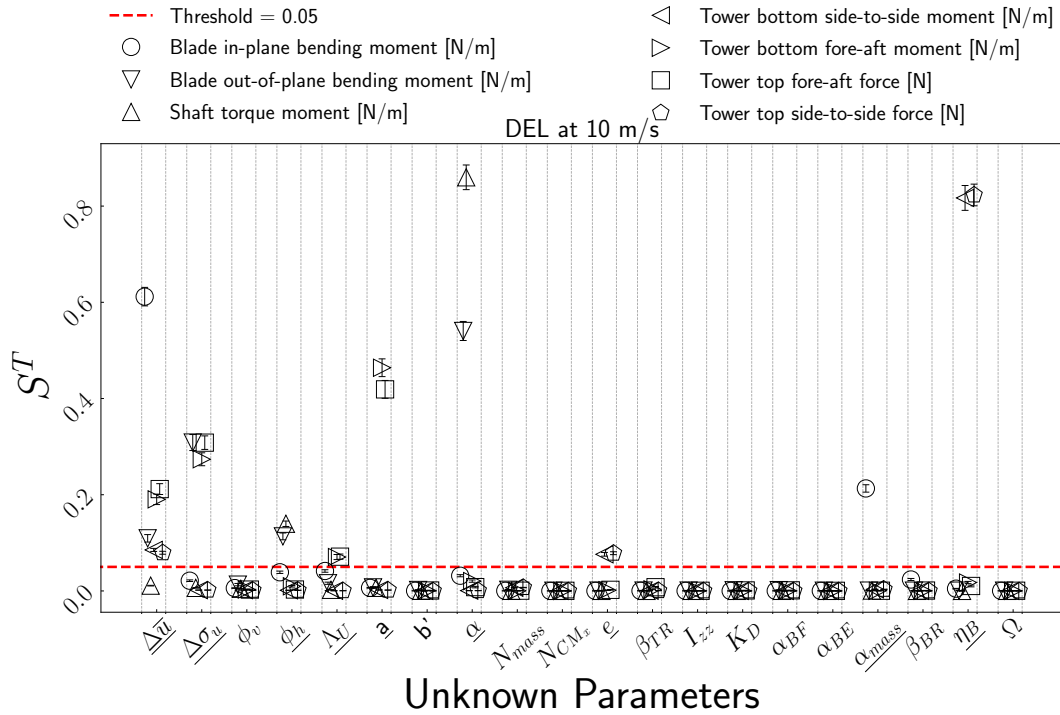


Figure 4. Estimation of total Sobol' indices (y-axis) with their 95% confidence interval corresponding to each of the 20 parameters (x-axis) for the different fatigue loads. The dashed line corresponds to a threshold arbitrarily chosen to $5.0e-2$. Underlined total Sobol' indices represent indices higher to the threshold value. Confidence intervals (CI) are obtained by taking into account the uncertainties due to both the metamodel and the Monte Carlo estimation. The number of samples for the conditional Gaussian process, in order to quantify the uncertainty of the kriging approximation, was set to 100. The uncertainty due to Monte Carlo integration was computed with a bootstrap procedure with a sample size of 100.

430

431

432 C. Identifiability study

433 A major issue for parameter estimation problem is the identifiability. In this context, Dobre
 434 *et al.* (2012) highlights that nullity of total sensitivity index for a specific input parameter implies
 435 its non-identifiability from the measured output used during the recursive inference procedure.
 436 Consequently, we perform a GSA on the measured outputs in order to determine which parameters
 437 cannot be inferred with the current sensors on the wind turbine. In our industrial application, six
 438 measured outputs are considered, see Table VI.

439 For the acceleration outputs, we are mainly interested in their response in the frequency-domain

440 by using the power spectral density (PSD). When performing GSA, discretized PSD series involve
 441 a substantial dimensionality and a high degree of redundancy. To overcome this issue, the different
 442 discretized PSD outputs have been reduced using a Principal Component Analysis (PCA) (Wold,
 443 Esbensen, and Geladi, 1987). This dimensionality reduction approach allows the functional output
 444 expansion in a new reduced space spanned by the most significant directions in terms of variance.
 445 Then, a method based on PCA and GSA with a GP model is used to compute an aggregated
 446 Sobol' index for each input parameter of the model. Indeed, the multivariate sensitivity analysis
 447 decomposes the discretized output into the non-correlated principal components and computes
 448 sensitivity indices on each principal component. Finally, the overall effect of each parameter can
 449 be summarized by the aggregated Sobol' index equal to the weighted sum of the indices over
 450 the principal component, with weights proportional to the inertia associated with the components
 451 (Lamboni, Monod, and Makowski, 2011).

452 The proposed index synthesizes the influence of the parameter on the whole discretized func-
 453 tional output. Table VII summarizes the estimated Sobol' indices for the scalar 10-minutes average
 454 observations and aggregated Sobol' indices for the discretized PSD series. In this sensitivity anal-
 455 ysis, the input parameters having total Sobol' index values under a threshold set at $1e - 02$ are
 456 considered as non-identifiable from the measured output.

Table VI. Observations from our reference wind turbine used in the data assimilation procedure.

Observation	Unit
10-minute mean power production	[kW]
10-minute mean rotor speed	[rpm]
Tower middle fore-aft acceleration's PSD	[dB]
Tower middle side-to-side acceleration's PSD	[dB]
Tower top fore-aft acceleration's PSD	[dB]
Tower top side to side acceleration's PSD	[dB]

457
458

Table VII. Total Sobol' and aggregated Sobol' indices for each output used during the recursive inference procedure. Due to the GSA on fatigue loads, the eight wind parameters have been whittled down to six, and the twelve model parameters have been whittled down to three. Estimated Sobol' indices higher than the arbitrary threshold, set at $1e - 02$, are underlined.

Measured output		$\overline{\Delta u}$ [m/s]	$\Delta \sigma_u$ [m/s]	ϕ_h [°]	Λ_u [m]	a [-]	α [-]	e [%]	α_{mass} [%]	η_B [%]
Sobol' index	10-minute mean power production	<u>9.81e-01</u>	4.29e-04	<u>1.71e-02</u>	1.30e-04	3.70e-04	<u>1.50e-02</u>	3.84e-05	3.83e-04	5.23e-05
	10-minute mean rotor speed	<u>9.75e-01</u>	3.30e-03	<u>1.87e-02</u>	9.43e-04	1.61e-03	<u>1.62e-02</u>	1.03e-04	7.56e-04	7.34e-05
Aggregated Sobol' index	Tower middle fore-aft acceleration's PSD	<u>1.44e-01</u>	<u>2.49e-01</u>	<u>1.00e-02</u>	<u>1.77e-01</u>	<u>3.70e-01</u>	<u>1.33e-02</u>	<u>4.58e-02</u>	5.82e-03	3.48e-03
	Tower middle side-to-side acceleration's PSD	<u>2.04e-01</u>	<u>2.51e-01</u>	<u>1.09e-02</u>	<u>1.92e-01</u>	<u>3.00e-01</u>	<u>1.33e-02</u>	<u>4.49e-02</u>	4.86e-03	3.42e-03
	Tower top fore-aft acceleration's PSD	<u>3.12e-01</u>	<u>2.16e-01</u>	<u>1.87e-02</u>	<u>1.75e-01</u>	<u>2.69e-01</u>	9.59e-03	<u>3.36e-02</u>	8.49e-03	7.01e-03
	Tower top side to side acceleration's PSD	<u>2.84e-01</u>	<u>1.87e-01</u>	<u>1.18e-02</u>	<u>1.76e-01</u>	<u>2.50e-01</u>	<u>1.21e-02</u>	<u>8.33e-02</u>	5.52e-03	<u>2.38e-02</u>

460 According to the GSA, the coefficient related to the blade mass coefficient α_{mass} is not identi-
461 fiable with the current observations. Consequently, the model parameter properties remaining for
462 the inference procedure are the tower thickness coefficient e , and the mass imbalance factor η_B .
463 Moreover, all the influent parameters related to the wind field remain candidates for the recursive
464 inference strategy.

465 D. Recursive inference strategy based on AnEnKF approach

466 The current in situ wind data availability or quality from the LIDAR system does not allow a
467 proper extraction of the mean flow angle ϕ_h , the longitudinal turbulence length scale Λ_u , and the
468 decrement parameter of the coherence model a . Consequently, only the five remaining parameters
469 having an influential effect on the fatigue behavior of the structure and potentially identifiable are
470 considered during the recursive inference procedure. These input parameters and their correspond-
471 ing prior Gaussian distributions are detailed in Table VIII. Their corresponding reference variable
472 in the augmented state vector is also specified.

473 For assessing the performance of the AnEnKF for our recursive inference procedure, we rely
474 on pseudo-experimental numerical tests. They consist in performing forward aero-servo-elastic
475 simulations considering known values of the input parameters, and then adding a Gaussian noise
476 of known variance to the simulated measurements. In our study, the simulated data are perturbed
477 by considering a covariance matrix such as the obtained standard deviation is equivalent to a 10%
478 signal-to-noise ratio. The pseudo-simulated responses of the wind turbine structure are generated

Table VIII. A-priori Gaussian distribution \mathcal{G} for each of the considered input parameters.

Input parameter	Variable	Distribution	Initial prior	State
Tower thickness	e	\mathcal{G}	$\mu = 0.00 \quad \sigma = 7.00e - 01$	\mathbf{x}^1
Blade mass imbalance	η_B	\mathcal{G}	$\mu = 2.50e - 02 \quad \sigma = 8.33e - 03$	
Error mean of the wind speed at hub height	$\Delta\bar{u}$	\mathcal{G}	$\mu = 0.00 \quad \sigma = 9.11e - 01$	\mathbf{x}^2
Error standard deviation of the wind speed at hub height	$\Delta\sigma_u$	\mathcal{G}	$\mu = 0.00 \quad \sigma = 9.70e - 02$	
Vertical wind shear exponent	α	\mathcal{G}	$\mu = 1.30e - 01 \quad \sigma = 2.90e - 01$	

479 using the wind inflow conditions obtained from the nacelle mounted LIDAR for a specific day and
480 the mean values of the model properties described in Table III. The noisy pseudo-experimental
481 outputs used to recursively update the wind turbine model are 10-minute mean power production
482 and rotor speed, and the PSD of the acceleration time series obtained for side to side and fore-
483 aft at the two different tower positions. Our recursive inference problem using a filtering-based
484 estimation procedure can be considered as a state estimation problem for the following augmented
485 system:

$$486 \quad \forall k \in \mathbb{N}^*, \begin{cases} \mathbf{x}^{(k)} = \begin{bmatrix} \mathbf{x}^1_{(k)} \\ \mathbf{x}^2_{(k)} \end{bmatrix} = \begin{pmatrix} \mathbf{x}^1_{(k-1)} \\ \mathcal{A}_{(k-1,k)}(\mathbf{x}^2_{(k-1)}) \end{pmatrix} + \boldsymbol{\varepsilon}^m_{(k)} \\ \mathbf{y}^{(k)} = \mathcal{H}_{(k)}(\mathbf{x}^{(k)}, \mathbf{v}^{(k)}) + \boldsymbol{\varepsilon}^o_{(k)} \end{cases} .$$

487 where $\mathbf{x}^1_{(k-1)}$ and $\mathbf{x}^2_{(k-1)}$ are respectively [the whittled-down set of five](#) uncertain parameters for
488 the model properties and the wind inflow conditions at iteration $k - 1$ as described in Table VIII,
489 $\mathcal{A}_{(k-1,k)}$ is the analog forecasting operator as detailed in Section III, $\mathbf{v}^{(k)}$ is the forcing vector cor-
490 responding to the 10-minute mean and standard deviation wind speed obtained from the SCADA
491 system, and $\mathcal{H}_{(k)}$ is the combination of the aero-servo-elastic model FAST and the turbulent wind
492 field generation software TurbSim.

493 For the initialization of the EnKF approach, independent Gaussian distributions are assumed
494 to be the initial prior for each of the input parameters, see Table VIII. The initial error covariance
495 matrix of the input parameters, denoted by P_b , is thus assumed to be diagonal. To create the
496 catalog, we rely on the measurements obtained from both the SCADA system and the LIDAR
497 installed on the onshore wind turbine. A data pretreatment has been performed in order to find
498 any corrupted observations. The obtained database consists in both 4,735 analog situations to be

499 compared to the current parameters related to the wind inflow and their corresponding successors
 500 at a 10-minute interval.

501 Figure 5 shows the results of the identification of the considered input parameters by applying
 502 the AnEnKF approach with the locally-linear forecasting operator using $N = 500$ members and
 503 $K = 50$ nearest-neighbors. It can be noticed that the augmented state vector is well reconstructed
 504 by using this non-parametric data assimilation procedure which allows to emulate the dynamical
 505 model from a dataset. Indeed, the mean of the empirical distribution obtained from the members
 506 of the ensemble is close to the true hidden-state for every parameter. A major advantage of the
 507 procedure is the confidence intervals obtained at each inference iteration allowing us to give infor-
 508 mation about the difficulty to retrieve the value of the input parameters from the measured outputs.
 509 We can notice that the uncertainties, represented by the ensemble, have drastically reduced trough
 510 the iterations. The confidence intervals take into account the errors related to the model and the
 511 observations.

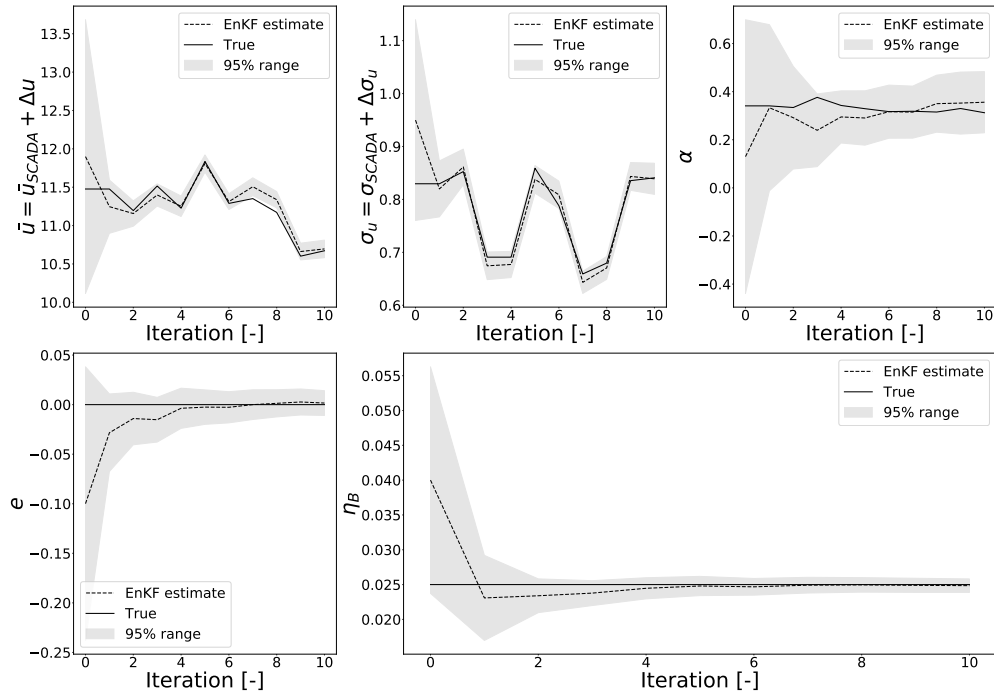


Figure 5. Iteration evolution of the posteriori estimates of the input parameters. Results obtained by running the AnEnKF procedure with $N = 500$ members of the ensemble used for the estimation and considering pseudo-experimental numerical observations.

512 V. CONCLUSION

513 In the present work, we extend a procedure to quantify and reduce the uncertainties affecting
514 the fatigue load estimation of a wind turbine numerical model. The fatigue loads encountered by a
515 wind turbine structure are function of the parameters describing the turbulent wind field, the struc-
516 tural properties, and the control system. The study aims at taking into account these parameters
517 used as input to aero-servo-elastic fatigue load simulations of an operating wind turbine. The pro-
518 cedure relies on a global sensitivity analysis and a recursive Bayesian inference method. A major
519 challenge during the recursive inference procedure is the dynamic behavior of the inflow-related
520 parameters. Unfortunately, the underlying dynamic behavior of these parameters is not explicitly
521 known. To overcome this issue, a combination of the implicit analog forecasting of the dynamics
522 with the ensemble Kalman filtering scheme is investigated.

523 Finally, we demonstrate the applicability and performance of the procedure using a numerical
524 representation of a reference wind turbine. The study leads to the following main conclusions.
525 The global sensitivity analysis based on heteroscedastic Gaussian processes for the estimation of
526 Sobol' indices shows that parameters related both to the wind and the structure have an influ-
527 ence on the fatigue loads of a wind turbine structure. The presented metamodeling approach is
528 an efficient way to capture the inherent stochasticity of aero-servo-elastic simulations due to the
529 turbulent inflow realization leading to variations in the quantities of interest. After determining the
530 most influential parameters in terms of fatigue loads variability, an identifiability study based on a
531 global sensitivity analysis is performed to assess if these parameters can be inferred from the cur-
532 rent sensors. The sensitivity analysis is based on the estimation of the so-called aggregated Sobol'
533 indices involving a principal component analysis in order to take into account the functional be-
534 havior of the measured outputs. Finally, the ensemble Kalman filtering method coupled with the
535 analog forecasting strategy used in this study is very suitable for carrying the recursive inference
536 of parameters related to the wind field solicitation and the wind turbine numerical description.

537 Further research should focus on the quality of the catalog used for the analog forecasting strat-
538 egy. Additionally, other types of kernels in the forecasting operator have to be studied. Lastly, the
539 hyperparameters used in the K -nearest neighbors method and the chosen kernel function could be
540 optimized for each member of the ensemble Kalman filtering procedure by using a cross-validation
541 approach. From an industrial perspective, the proposed AnEnKF methodology has to be performed
542 using measured acceleration time-series obtained from the sensor devices of the onshore wind tur-

543 bine.

544 **ACKNOWLEDGMENTS**

545 The author acknowledge SMARTEOLE project partners for the use of experimental data from
546 national project SMARTEOLE (ANR-14-CE05-0034) measurement campaigns.

REFERENCES

- Aanonsen, S. I., Nævdal, G., Oliver, D. S., Reynolds, A. C., Vallès, B., *et al.*, “The ensemble kalman filter in reservoir engineering—a review,” *Spe Journal* **14**, 393–412 (2009).
- Alexander, R., Zhao, Z., Székely, E., and Giannakis, D., “Kernel analog forecasting of tropical intraseasonal oscillations,” *Journal of the Atmospheric Sciences* **74**, 1321–1342 (2017).
- Ayet, A. and Tandeo, P., “Nowcasting solar irradiance using an analog method and geostationary satellite images,” *Solar Energy* **164**, 301–315 (2018).
- Bertino, L., Evensen, G., and Wackernagel, H., “Sequential data assimilation techniques in oceanography,” *International Statistical Review* **71**, 223–241 (2003).
- Bocquet, M., Farchi, A., and Malartic, Q., “Online learning of both state and dynamics using ensemble kalman filters,” arXiv preprint arXiv:2006.03859 (2020).
- Brown, S. D., “The kalman filter in analytical chemistry,” *Analytica chimica acta* **181**, 1–26 (1986).
- Brunton, S. L., Proctor, J. L., and Kutz, J. N., “Discovering governing equations from data by sparse identification of nonlinear dynamical systems,” *Proceedings of the national academy of sciences* **113**, 3932–3937 (2016).
- Chau, T. T. T., Ailliot, P., and Monbet, V., “An algorithm for non-parametric estimation in state–space models,” *Computational Statistics & Data Analysis* **153**, 107062 (2021).
- Chen, L., “Curse of dimensionality,” in *Encyclopedia of Database Systems*, edited by L. LIU and M. T. ÖZSU (Springer US, Boston, MA, 2009) pp. 545–546.
- Damblin, G., Couplet, M., and Iooss, B., “Numerical studies of space-filling designs: optimization of latin hypercube samples and subprojection properties,” *Journal of Simulation* **7**, 276–289 (2013).
- Dimitrov, N., Natarajan, A., and Kelly, M., “Model of wind shear conditional on turbulence and its impact on wind turbine loads,” *Wind Energy* **18**, 1917–1931 (2015).
- Dimitrov, N., Natarajan, A., and Mann, J., “Effects of normal and extreme turbulence spectral parameters on wind turbine loads,” *Renewable Energy* **101**, 1180–1193 (2017).
- Dobre, S., Bastogne, T., Profeta, C., Barberi-Heyob, M., and Richard, A., “Limits of variance-based sensitivity analysis for non-identifiability testing in high dimensional dynamic models,” *Automatica* **48**, 2740–2749 (2012).
- Durbin, J. and Koopman, S. J., *Time series analysis by state space methods* (Oxford university press, 2012).

- Efron, B., “Nonparametric estimates of standard error: the jackknife, the bootstrap and other methods,” *Biometrika* **68**, 589–599 (1981).
- Evensen, G., “Sequential data assimilation with a nonlinear quasi-geostrophic model using monte carlo methods to forecast error statistics,” *Journal of Geophysical Research: Oceans* **99**, 10143–10162 (1994).
- Evensen, G., “The ensemble kalman filter: Theoretical formulation and practical implementation,” *Ocean dynamics* **53**, 343–367 (2003).
- Evensen, G., *Data assimilation: the ensemble Kalman filter* (Springer Science and Business Media, 2009).
- Fablet, R., Viet, P., Lguensat, R., and Chapron, B., “Data-driven assimilation of irregularly-sampled image time series,” in *2017 IEEE International Conference on Image Processing (ICIP)* (IEEE, 2017) pp. 4302–4306.
- Friedman, J. H., “On bias, variance, 0/1-loss, and the curse-of-dimensionality,” *Data mining and knowledge discovery* **1**, 55–77 (1997).
- Ginsbourger, D., Picheny, V., Roustant, O., and Richet, Y., “Kriging with heterogeneous nugget effect for the approximation of noisy simulators with tunable fidelity (krigeage avec effet de pépite hétérogène pour l’approximation de simulateurs bruités à fidélité réglable),” (2008).
- Hamilton, F., Berry, T., and Sauer, T., “Ensemble kalman filtering without a model,” *Physical Review X* **6**, 011021 (2016).
- Hansen, M., *Aerodynamics of wind turbines* (Routledge, 2015).
- Harvey, A. C., *Forecasting, structural time series models and the Kalman filter* (Cambridge university press, 1990).
- Haykin, S., *Kalman filtering and neural networks*, Vol. 47 (John Wiley & Sons, 2004).
- Hirvoas, A., Prieur, C., Arnaud, E., Caleyron, F., and Munoz Zuniga, M., “Quantification and reduction of uncertainties in a wind turbine numerical model based on a global sensitivity analysis and a recursive bayesian inference approach,” *International Journal for Numerical Methods in Engineering* (2021), <https://doi.org/10.1002/nme.6630>, <https://onlinelibrary.wiley.com/doi/pdf/10.1002/nme.6630>.
- Holierhoek, J., Korterink, H., van de Pieterman, R., Rademakers, L., and Lekou, D., “Recommended Practices for Measuring in Situ the ‘Loads’ on Drive Train, Pitch System and Yaw System.” Energy Research Center of the Netherlands (ECN) (2010).
- Houtekamer, P. L., He, B., and Mitchell, H. L., “Parallel implementation of an ensemble kalman

- filter,” *Monthly Weather Review* **142**, 1163–1182 (2014).
- Houtekamer, P. L. and Mitchell, H. L., “A sequential ensemble kalman filter for atmospheric data assimilation,” *Monthly Weather Review* **129**, 123–137 (2001).
- IEC, I. E. C., “Iec 61400-1: 2019: Wind energy generation systems-part 1: Design requirements,” (2019).
- Iooss, B., Janon, A., Pujol, G., with contributions from Baptiste Broto., Boumhaout, K., Veiga, S. D., Delage, T., Fruth, J., Gilquin, L., Guillaume, J., Le Gratiet, L., Lemaitre, P., Nelson, B. L., Monari, F., Oomen, R., Rakovec, O., Ramos, B., Roustant, O., Song, E., Staum, J., Sueur, R., Touati, T., and Weber, F., *sensitivity: Global Sensitivity Analysis of Model Outputs* (2019), r package version 1.16.0.
- Jansen, M. J., “Analysis of variance designs for model output,” *Computer Physics Communications* **117**, 35–43 (1999).
- Jonkman, B. J., “Turbsim user’s guide: Version 1.50,” Tech. Rep. (National Renewable Energy Lab (NREL), Golden, CO, USA, 2009).
- Jonkman, J. M. ., Buhl Jr., M. L., *et al.*, “Fast user’s guide,” Golden, CO: National Renewable Energy Laboratory **365**, 366 (2005).
- Julier, S. J. and Uhlmann, J. K., “New extension of the kalman filter to nonlinear systems,” in *Signal processing, sensor fusion, and target recognition VI*, Vol. 3068 (International Society for Optics and Photonics, 1997) pp. 182–193.
- Kaimal, J. C., Wyngaard, J. C., Izumi, Y., and Coté, O., “Spectral characteristics of surface-layer turbulence,” *Quarterly Journal of the Royal Meteorological Society* **98**, 563–589 (1972).
- Kalman, R. E., “A new approach to linear filtering and prediction problems,” (1960).
- Koukoura, C., *Validated Loads Prediction Models for Offshore Wind Turbines for Enhanced Component Reliability*, Ph.D. thesis, Technical University of Denmark (2014).
- Lamboni, M., Monod, H., and Makowski, D., “Multivariate sensitivity analysis to measure global contribution of input factors in dynamic models,” *Reliability Engineering and System Safety* **96**, 450–459 (2011).
- Lguensat, R., Tandeo, P., Ailliot, P., Pulido, M., and Fablet, R., “The analog data assimilation,” *Monthly Weather Review* **145**, 4093–4107 (2017).
- Lorenz, E. N., “Atmospheric predictability as revealed by naturally occurring analogues,” *Journal of the Atmospheric sciences* **26**, 636–646 (1969).
- Marrel, A., Iooss, B., Van Dorpe, F., and Volkova, E., “An efficient methodology for modeling

- complex computer codes with gaussian processes,” *Computational Statistics and Data Analysis* **52**, 4731–4744 (2008).
- Meyers, M. A. and Chawla, K. K., *Mechanical behavior of materials* (Cambridge university press, 2008).
- Pathak, J., Hunt, B., Girvan, M., Lu, Z., and Ott, E., “Model-free prediction of large spatiotemporally chaotic systems from data: A reservoir computing approach,” *Physical Review Letters* **120** (2018), 10.1103/PhysRevLett.120.024102.
- Peterson, L. E., “K-nearest neighbor,” *Scholarpedia* **4**, 1883 (2009).
- Robertson, A. N., Shaler, K., Sethuraman, L., and Jonkman, J. M., “Sensitivity analysis of the effect of wind characteristics and turbine properties on wind turbine loads,” *Wind Energy Science* (Online) **4** (2019a).
- Robertson, A. N., Shaler, K., Sethuraman, L., and Jonkman, J. M., “Sensitivity of uncertainty in wind characteristics and wind turbine properties on wind turbine extreme and fatigue loads,” *Wind Energy Science Discussions* , 1–41 (2019b).
- Saranyasontorn, K., Manuel, L., and Veers, P., “On estimation of coherence in inflow turbulence based on field measurements,” in *42nd AIAA Aerospace Sciences Meeting and Exhibit* (2004) p. 1002.
- Simms, D., Schreck, S., Hand, M., and Fingersh, L. J., “Nrel unsteady aerodynamics experiment in the nasa-ames wind tunnel: a comparison of predictions to measurements,” *Tech. Rep.* (National Renewable Energy Lab., Golden, CO (US), 2001).
- Snyder, C. and Zhang, F., “Assimilation of simulated doppler radar observations with an ensemble kalman filter.” *Monthly Weather Review* **131** (2003).
- Sobol’, I. M., “On sensitivity estimation for nonlinear mathematical models,” *Matematicheskoe modelirovanie* **2**, 112–118 (1990).
- Solari, G. and Piccardo, G., “Probabilistic 3-d turbulence modeling for gust buffeting of structures,” *Probabilistic Engineering Mechanics* **16**, 73–86 (2001).
- Tandeo, P., Ailliot, P., Fablet, R., Ruiz, J., Rousseau, F., and Chapron, B., “The analog ensemble kalman filter and smoother,” (2014).
- Tandeo, P., Ailliot, P., Ruiz, J., Hannart, A., Chapron, B., Cuzol, A., Monbet, V., Easton, R., and Fablet, R., “Combining analog method and ensemble data assimilation: application to the lorenz-63 chaotic system,” in *Machine learning and data mining approaches to climate science* (Springer, 2015) pp. 3–12.

- Toth, Z., “Long-range weather forecasting using an analog approach,” *Journal of climate* **2**, 594–607 (1989).
- Veldkamp, H. F., “Chances in wind energy: a probabilistic approach to wind turbine fatigue design,” (2006).
- Welch, P., “The use of fast fourier transform for the estimation of power spectra: a method based on time averaging over short, modified periodograms,” *IEEE Transactions on audio and electroacoustics* **15**, 70–73 (1967).
- Wells, C., *The Kalman filter in finance*, Vol. 32 (Springer Science and Business Media, 2013).
- Witcher, D., “Uncertainty Quantification Techniques in Wind Turbine,” (2017).
- Wold, S., Esbensen, K., and Geladi, P., “Principal component analysis,” *Chemometrics and intelligent laboratory systems* **2**, 37–52 (1987).